Production of muon pairs in K^0_L-Cu interactions

M. Faessler,* J. Kirkby, J. Liu,† and S. Wojcicki
Stanford Linear Accelerator Center
and Physics Department, Stanford University, Stanford, California 94305

R. Burns,‡ P. Condon, and P. Cowell§
University of California, Irvine, California 92664
(Received 25 July 1977)

The dimuon production mass spectrum has been measured with a beam of 4–20-GeV/c K^0_L's incident on a copper target. The production of $\mu^+\mu^-$ pairs resulting from the decay of vector mesons (ρ, ω, and ϕ) was observed with a cross section of 55 ± 10 nb per nucleon for $x_F > 0.25$ based on a specific production model. In addition we measured upper limits for $\mu^+\mu^-$ pair production cross sections with $x_F > 0.25$ of 20 nb per nucleon for $m_{\mu\mu} < 0.5$ GeV/c^2 and 35 nb per nucleon at the $\psi(3100)$.

I. INTRODUCTION

The studies of direct muon production in hadronic interactions originated about 15 years ago with experiments by the Columbia-BNL and Wisconsin-ANL groups, with both searches yielding negative results.[1] We use the word "direct muons" to denote those muons which do not come from conventional processes such as π, K, or hyperon decay, or Bethe-Heitler conversions of photons into muon pairs in the target material. The search for muons was motivated at that time principally by the fact that a high-transverse-momentum (P_T) muon might be a signature of intermediate-vector-boson production in hadronic processes, i.e.,

$$p + p_1 \rightarrow W^{\pm} + \text{hadrons},$$

followed by

$$W^{\pm} \rightarrow \mu^{\pm} + \nu_{\mu}.$$

It was pointed out subsequently by Yamaguchi[2] that the production of W bosons must be related by conserved vector current (CVC) to the production of heavy virtual photons, which could subsequently decay to muon pairs. This process would contribute to the high-P_T muons and thereby obscure their interpretation.

The first published observation of direct muons was made by the Yale-BNL group[3] which also measured muon polarization in order to isolate the potential W-boson signal from the muons of electromagnetic origin. No evidence was found for W production. Concurrently, Lederman and his collaborators performed[4] the first extensive study of dimuons from hadronic interactions, observing muon pairs up to masses of 6.7 GeV/c^2.

More recently the question of direct muons has been the focus of extensive experimental and theoretical attention. A calculation of the hadron-constitutent-annihilation process by Drell and Yan[5] anticipated a substantial production of direct lepton pairs. Shortly afterwards, both direct muons and electrons were observed in hadronic interactions at Fermilab with a lepton-pion ratio approximately constant at about 10^{-4} over a wide range of P_T and incident energies.[6] The observed rate was too large to be accommodated by vector-meson production followed by decay into lepton pairs and the Drell-Yan mechanism with a conventional parton distribution. The subsequent discovery of the ψ/J (Ref. 7) and ψ' (Ref. 8) provided another source of direct leptons, especially at large values of P_T, but the contribution proved insufficient to remove the discrepancy.[9]

The possibility was raised of a new source such as a heavy lepton or hadron with a new quantum number. A candidate for the latter was charm[10] which had been introduced to account for the low rate observed in the decay $K^0_L \rightarrow \mu^+\mu^-$. Charmed particles decay weakly and were expected to have branching ratios to leptons of approximately 10%.

More recently, Farrar and Frautschi[11] pointed out that the existing data were not incompatible with production of single photons with a copious rate of 1–10% of the pions. An excess of photons (above that expected from π^0 and η decay) was indeed observed[12] at the CERN ISR in the P_T range between 3 and 4 GeV/c.

The electromagnetic, as opposed to weak, origin for direct leptons in hadronic interactions has received support from two experiments at Fermilab which compared dimuon yield with the inclusive single-muon yield.[13] They found the (observed) single muons were consistent with originating entirely in dimuon pairs. On the other hand, a contribution at the level of 20–25% from sources other than dimuons could not be excluded. A contradictory conclusion was reached by a group working at lower energies at Serpukhov which found a μ^+/μ^- ratio of 1.21.[14]

Further contradictions exist in measurements of muon polarization. The Yale group working at Fermilab found polarization consistent with zero,[15] both at low values of P_T and at a mean P_T of 2.15 GeV/c, and thereby supported the concept of electromagnetic origin. The Serpukhov group, however, found a nonzero polarization at high values of P_T (Ref. 16) consistent with the dominant source being a weak decay of a new hadron via a $V+A$ current. A more recent measurement[17] by the Yale-BNL group found no polarization of muons produced by 28.5-GeV protons at a $P_T \sim 2$ GeV/c.

Further experiments have explored this production process in different domains of s and P_T,[18] or reanalyzed old data to extract the prompt lepton signals.[19]

We will briefly summarize the present understanding of direct leptons and refer the reader to review talks[20] for details.

It is well established that the lepton-pion ratio is $\sim 10^{-4}$ over a wide range of kinematical variables, with a decrease at high x values. In addition, there are strong indications that the e/π ratio increases as P_T decreases.[21] There is some experimental uncertainty where the threshold exists for direct lepton production.[22]

There is now good evidence[23] for the existence of a dimuon continuum in addition to the muon pairs from vector-meson decays. In particular the low-mass dilepton cross section seems to be larger than that expected from radiative decays of η and ω mesons.

With the discovery of charmed particles[24] and the observation of their semileptonic (or possibly purely leptonic) decay modes in both neutrino[25] and e^+e^- colliding-beam[26] experiments, it is clear that they contribute to the direct lepton signal observed in hadronic collisions. So far, however, all the direct searches for charmed particles in hadronic interactions are negative,[27] so the size of this contribution remains unknown.

This experiment contributes to the subject a measurement of muon pair production by K_L^0 interactions at intermediate energies and a study of the expected sources. At these energies the large background of muons generated by π/K decays excludes single-muon measurements.

II. APPARATUS

The experiment was carried out at the Stanford Linear Accelerator Center using a modified version of the K_L^0 Spectrometer Facility as shown in Fig. 1. A total of seven absorption lengths (λ) of Cu, consisting of 14 slabs of Cu, each 80 cm × 40 cm × 7.5 cm, was positioned in the path of the K_L^0 beam which itself was 60 cm × 30 cm in area. The

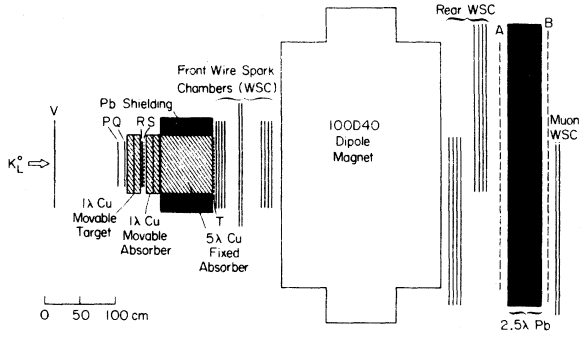

FIG. 1. Plan view of apparatus.

first interaction length of Cu represented the target, while the next six constituted the front hadron absorber. The first four slabs in this assembly were movable along the beam direction, allowing us to vary the effective density of that portion of the target-absorber material which was most significant from the point of view of pion decays. We ran with 0-, 4-, and 8-cm air gaps between these slabs, and shall refer to these data as 0-, 4-, and 8-cm data. Additional Pb shielding was stacked around the Cu absorber to cut down the wide-angle hadrons.

A 75 cm × 45 cm veto counter V was placed about 2 m upstream of the target to define the decay region for $K_{\mu 3}^0$ decays. When accompanied by the subsequent decay $\pi \to \mu\nu$ these events provided the flux measurement for the experiment. The downstream limit of the decay region was defined by two banks of scintillation counters P and Q, each composed of six horizontal counters of dimension 60 cm × 5 cm × 0.3 cm. A similar horizontal bank R and a 13-counter vertical bank S were positioned between the Cu target and the absorber, and a 17-counter vertical bank T was placed behind the Cu absorber. Both the S and T counters were of the same size as the P, Q, and R counters. The T counter bank was followed by 10 planes ($4X$, $4Y$, U, and V) of capacitive-readout wire spark chambers, followed by a 100D40 dipole analyzing magnet. The magnetic field was constantly monitored by a nuclear-magnetic-resonance (NMR) probe and had a typical $\int Bdl$ value of 12.6 kG m. Two separate groups of wire chambers, each consisting of $2X$ and $2Y$ readout planes, were arranged behind the magnet in such a way as to cover the maximum solid angle. A bank of 23 vertical 15 cm × 168 cm × 1.25 cm A counters were positioned before a 2.5 absorption length Pb absorber, followed by a similar bank of 25 vertical B counters. Behind the B counters, on one side of the spectrometer, were two large wire chambers which were

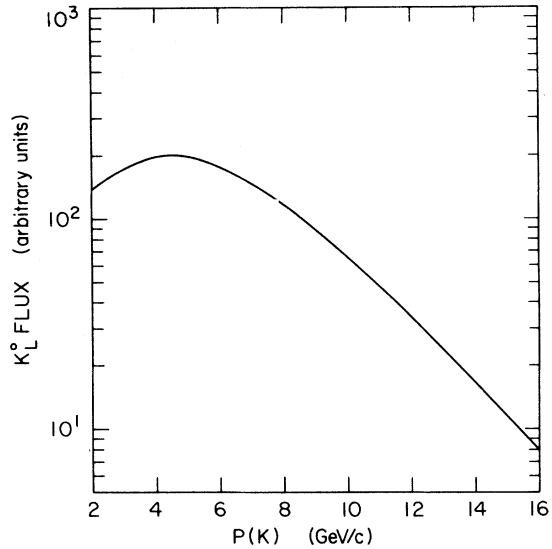

FIG. 2. The incident K_L^0 momentum spectrum at the Cu target.

used to measure the X and Y coordinates of muons which penetrated the Pb wall. These will be referred to as the "muon WSC's."

The V counter was viewed by two 56AVP phototubes at each end, while the P, Q, R, S, and T counters each had a single 56AVP phototube. The A and B counters were viewed by XP1021 and 56AVP phototubes, respectively, one at each end of a counter. The anode signal from each phototube was discriminated and the discriminator output fed into both latch and time-of-flight (TOF) circuits, the latter having a typical sensitivity of 0.1 nsec/channel. In addition, all the discriminator outputs from each bank of counters were mixed to form overall trigger levels for each counter bank separately. Both the latch and TOF gates were generated by the output of the A mixer.

The experiment was run using a 3-mA primary SLAC electron beam of 21.5 GeV, with a neutral beam extracted at 1.5 degrees off a 1-radiation-length (rl) Be target. In order to cut down the gamma component in this beam, 58 rl of Pb were placed in the beam before the first collimator. Likewise, in order to improve the K_L^0 to neutron ratio, 1.5 collision lengths of polyethylene were introduced just after the Pb absorber. Two sweeping magnets in the beam line eliminated charged particles from the beam. The K_L^0 spectrum at the spectrometer is shown in Fig. 2. A total flux of 5.6×10^9 K_L^0 was obtained during the experiment.

III. DATA ACQUISITION

Candidates for muons were required to traverse both the upstream Cu absorber and the downstream Pb absorber. Consequently, a $2T \cdot 2A \cdot 2B$ trigger was set up to select events with two muons in the final state. The three general classes of events of interest which satisfied this trigger were as follows:

(1) Interaction events in which the K_L^0 interacted in the Cu target resulting in the production of two muons. This category of events was composed of that subset of triggers which satisfied a $\bar{V} \cdot \bar{P} \cdot \bar{Q} \cdot R \cdot S \cdot 2T \cdot 2A \cdot 2B$ logical requirement.

(2) $K_{\mu 3}^0$ decay events in which the $K_L^0 \to \pi \mu \nu$ decay occurred in the decay region between V and P, followed by a subsequent $\pi \to \mu \nu$ decay. These decays were defined as events satisfying a $\bar{V} \cdot P \cdot Q \cdot R \cdot S \cdot 2T \cdot 2A \cdot 2B$ requirement.

(3) Upstream decays in which the $K_{\mu 3}^0$ decay occurred upstream of the veto counter. These events satisfied a $V \cdot P \cdot Q \cdot R \cdot S \cdot 2T \cdot 2A \cdot 2B$ requirement.

In addition, an alternate single-muon trigger $V \cdot T \cdot A \cdot B$ was also set up to record events with a single upstream muon.

When an event trigger was satisfied, the latch, TOF, and wire-chamber data were written onto a magnetic tape for subsequent off-line analysis. In addition, the on-line PDP-9 computer was used to accumulate and display histograms in order to indicate experimental malfunctions.

The performance of the counters was monitored every 24 hours by pulsing light-emitting diodes (LED's) embedded in each of the counters. These LED runs were also used to provide calibration of each TOF unit. A single-muon run was then taken with the sweeping magnets off to allow beam muons to enter the apparatus. These runs were used to set the zero times for each TOF circuit. The performance of the wire spark chambers was also closely monitored throughout the experiment and multispark efficiencies in excess of 95% were observed in all the planes.

IV. DATA REDUCTION

The data-reduction techniques employed were similar to those used in the other experiments performed with this K_L^0 spectrometer and have been described in detail elsewhere.[28] Accordingly, we shall emphasize here only those features which were unique to this experiment. Firstly, the program searched for all the front and rear track segments in both the X and Y projections and then used the U V planes in the front, and A counters together with their TOF readings in the rear, to group these projections into spatial segments. Subsequently, the front and rear track segments were matched to form full tracks from which momenta were determined. A match was defined as

satisfactory if the front and rear segments crossed the midplane of the magnet within 7 cm. We estimate the efficiency for finding full tracks to be about 96%. Each full track was then checked to see if it satisfied a muon candidate criterion. As previously indicated, a minimum requirement for a muon track was that it triggered $R \cdot S \cdot T \cdot A \cdot B$. The front and rear segments of each muon candidate were projected through the counter banks and associated with latched counters. For example, at the A bank the projected position was compared with the X value of the center of the nearest A counter which fired, and with the Y in that counter as indicated by the difference in the TOF readings of the phototubes at either end of the counter. Expected X and/or Y deviations for each counter bank were determined experimentally as a function of track momentum, and these values were used as standard deviations to compute a contribution to an overall muon χ^2 at each counter bank. In addition, for the muon candidate to be accepted as a muon a minimum residual kinetic energy of 0.1 GeV was required at the downstream end of the Pb filter.

The TOF readings from the A and B counters associated with a muon candidate were averaged to give a reference time for that muon candidate. The TOF readings of corresponding counters in all other banks, after corrections for position in the counter, were compared to this reference time. Again, a momentum-dependent σ was obtained from the data for each counter bank and contributions to the muon χ^2 were computed for each counter bank. The overall muon χ^2 thus consisted of two components, one from the geometrical comparison and one from the TOF comparison.

For the muon candidate to be accepted as a muon for the subsequent analysis a $\chi^2 < 30$ or 40 was required depending upon whether it was an interaction ($\bar{V} \cdot \bar{P} \cdot \bar{Q} \cdot R \cdot S \cdot T \cdot A \cdot B$) or decay ($P \cdot Q \cdot R \cdot S \cdot T \cdot A \cdot B$) muon, respectively. The difference in the cutoff compensated for the extra contribution to the χ^2 of the P and Q counters necessary for the decay muons.

An average time for each muon track was derived by weighting the corrected TOF reading in each associated counter by $1/\sigma^2$, where σ was the appropriate standard deviation for that particular counter bank.

From the Fermi formula for multiple scattering,[29] it can be shown that the best estimate for the initial direction of a muon is

$$u = \tfrac{1}{2}(3\hat{u}_{\text{proj}} - \hat{u}_{\text{meas}}),$$

where $\hat{u}_{\text{meas}}$ is the measured direction in the front wire spark chambers, and $\hat{u}_{\text{prog}}$ is defined by the exit position of the track at the end of the Cu absorber and the location of the best-estimated interaction or decay point. For all muons, the X and Y of this production point were determined from the location of the associated P, Q, R, and S counters. The Z location of the origin of interaction and decay muons was taken to be the mean Z for interactions and decays respectively, while that for the upstream muons was taken to be 50 cm in front of the veto counter.

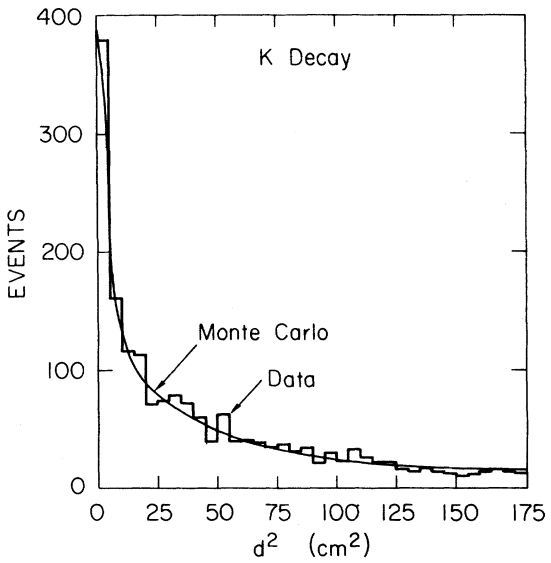

FIG. 3. Distribution of d^2, the square of the distance of closest approach for K decay events. The Monte Carlo distribution is shown for comparison.

The analysis program then proceeded to find all vertices between pairs of good muon tracks, using the best-estimate muon directions. Figure 3 shows the distribution in d^2, the square of the distance of closest approach between pairs of muon tracks in the final K decay data sample, together with the expected distribution calculated by a Monte Carlo technique. In addition, all possible vertices between a full track, not necessarily a muon, and an unmatched front track segment were also calculated for subsequent use in background subtraction (see below).

Finally, the candidates for good decay or interaction events were defined by the following criteria:

(1) two good full muon tracks,

(2) $|\text{TOF}(\mu^+) - \text{TOF}(\mu^-)| \leq 1.2$ nsec,

(3) satisfactory vertex, with $d^2 < 225$ cm^2.

The events passing these tests formed the raw sample of interaction, decay, or upstream decay candidates. The number of events in each of the three categories at this stage is enumerated in Table I.

TABLE I. Event candidates before VEND cut.

	Interaction	K decay	Upstream
+-	993	1949	5126
++/--	230	91	217

V. MONTE CARLO

A Monte Carlo simulation of the experiment was performed in order to determine the detection efficiency of the apparatus as a function of the mass of the produced dimuon pair, as well as the efficiency for observing $K_{\mu 3}^0$ decays. The differential cross section for $K_L^0+N\to\mu^+\mu^-X$ was taken to have the form

$$\frac{d^2\sigma}{dx_F dP_T^2}\propto(1-|x_F|)^3 e^{-4.2P_T^2}, \tag{1}$$

where P_T is the transverse momentum of the $\mu^+\mu^-$ pair and $x_F=P_\parallel^*/P_\parallel^{*\max}$ with $P_\parallel^*$ the longitudinal momentum of the muon pair in the K^0-nucleon center-of-mass system. This form was able to reproduce reasonably well the observed

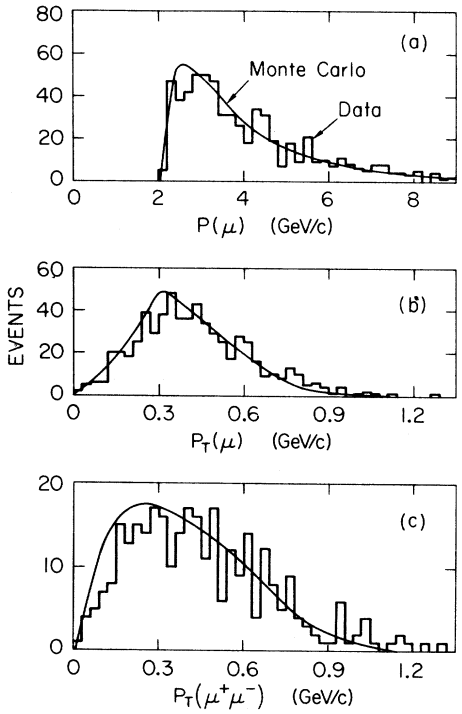

FIG. 4. Distribution of (a) muon momentum in the laboratory, (b) transverse momentum of muons, and (c) transverse momentum of the $\mu^+\mu^-$ pair for interaction events. The smooth line in each case denotes the expected distribution from Monte Carlo studies.

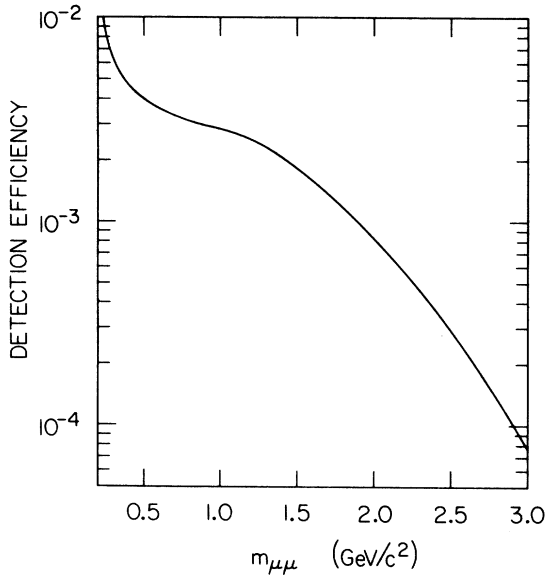

FIG. 5. Detection efficiency of the apparatus as a function of the dimuon mass produced in the reaction $K_L^0N\to\mu^+\mu^-X$, integrated over the K_L^0 momentum spectrum.

P_T and total energy distribution of the dimuon pairs in the vector-meson region, as illustrated in Fig. 4 where the actual data are compared with the Monte Carlo prediction. Full accounting of multiple scattering and ionization energy loss was included in the Monte Carlo calculation. The accepted events were subjected to an identical set of cuts as those applied to the data. The calculated relative efficiency of the spectrometer as a function of dimuon mass is shown in Fig. 5.

The calculated probability of the occurrence and detection of the process

$$K_L^0\to\pi\mu\nu,\ \pi\to\mu\nu$$

was 3.7×10^{-7} per incident K_L^0 averaged over the momentum spectrum of the incident beam. The form factors for $K_{\mu 3}^0$ decay were taken from Donaldson *et al.*[30]

VI. BACKGROUND SUBTRACTION

In this section we discuss the corrections and subtractions performed on the data in order to obtain a pure sample of muon pairs originating in the target region, i.e., between the Q and R target banks. These genuine target muon pairs consist not only of events of interest, i.e., dimuons produced in K_L^0 Cu interactions but also of $K\to\pi\mu\nu$ (followed by $\pi\to\mu\nu$) decays occurring in the target and Bethe-Heitler conversions into $\mu\mu$ pairs from secondary γ rays produced in K_L^0 Cu interaction. We shall estimate these residual

sources in the next section and discuss first the separation of an unbiased sample of target dimuons.

The possible sources of contamination can be grouped into five categories:

(1) K_L^0 interactions occurring near the downstream end of the copper absorber and giving rise to at least two tracks that satisfy the muon criterion.

(2) K_L^0 interactions in the absorber, downstream of the S counters, producing at least two tracks satisfying the muon criterion.

(3) pions produced in the target which simulated muons either by decaying before interacting, or by penetrating the whole length of the absorber.

(4) events with each of the muons coming from a different K_L^0 interaction, the two interactions being accidentally in time.

(5) K decays occurring upstream of the target region and giving rise to two muons with both the P and Q counter banks failing to register any counts.

The first two categories are not *a priori* distinct. The separation is important, however, because the majority of the events occurring near the downstream end of the copper absorber can be removed on an event-by-event basis (see discussion below), whereas the events originating from deep inside the absorber have to be removed on a statistical basis. We will discuss in more detail each of the five background sources and the procedures used to obtain the final sample of events.

(1) K_L^0 interactions near the downstream end of the absorber. The two dominant physical processes that contribute here are as follows:

(a) A K_L^0 interaction which triggers the R and S counters occurs accidentally in time with an interaction or decay of another K_L^0 near the downstream end of the absorber. The probability that a 1 GeV π produced at the end of the Cu block will register as a μ is non-negligible(12%). It can do so either by decaying in the 4 m of He in the magnet, or by punching through 46 cm of Pb between the A and B counters.

(b) A single K_L^0 first undergoes an interaction in the Cu target, leaving there a small part of its energy sufficient to trigger R and S counters. The same K_L^0 then penetrates almost to the end of the Cu absorber before interacting again or decaying. It is the products of this decay or second interaction which give rise to the two tracks which pass the subsequent muon criteria.

The sizable contribution from these two sources to the "interaction events" is illustrated in Fig. 6 where we display the Z distribution of the vertex point for the three categories of events of interest.

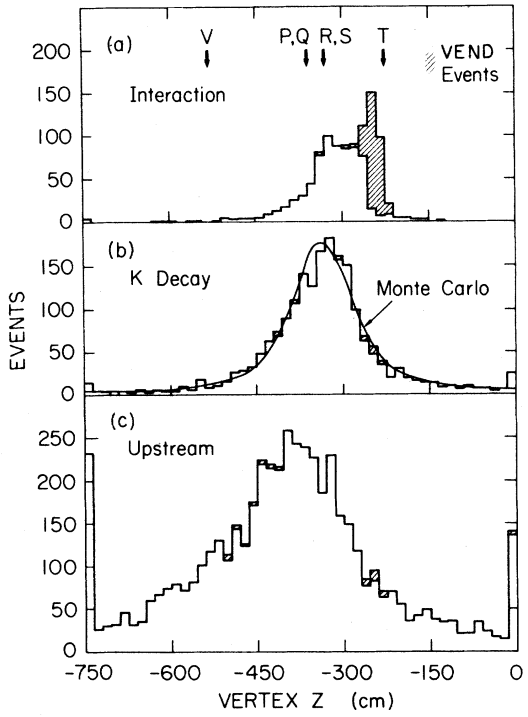

FIG. 6. Distribution in Z for (a) interaction vertices, (b) K decay vertices, and (c) upstream vertices. The locations of the front counter banks are shown. The slashed area represents the events which are eliminated by the VEND cut. The Monte Carlo distribution for (b) is also shown.

Whereas the two decay categories exhibit the expected distributions, the interaction events show an excess of events near the downstream end of the absorber. Additional evidence for this kind of background comes from the visual inspection of the events. While the decay events tend to be rather clean with essentially no sparks in addition to those associated with the two muons, the subset of the interaction events pointing to a vertex at the downstream edge of the Cu absorber shows a high multiplicity of tracks.

The sample of interaction events was purified by eliminating those events where at least one pair of (full + full) or (full + unmatched front) tracks gave a "very good" intersection near the end of the Cu absorber, with $d^2 < 5$ cm^2 and $-260 < Z < -220$ cm. We emphasize the "very good" as opposed to merely satisfactory requirement here. A low-mass dimuon system produced upstream in the target part of the absorber has a reasonable probability of giving a vertex near the downstream end of the absorber. But owing to the Coulomb scattering, the distance of closest approach will tend to be rather large in contrast with the tracks produced at the end of the copper. According to

TABLE II. Event candidates after VEND cut.

	Interaction	K decay	Upstream
+-	705	1908	5035
++/--	116	81	206

Monte Carlo calculation, the procedure used should be completely effective in removing the interactions at the end of the Cu block, with negligible loss of the events originating in the Cu target. The number of events remaining after this cut (referred to as VEND cut in the subsequent discussion) is shown in Table II and in Fig. 6.

(2) K_L^0 interactions in the upstream part of the absorber. Again, there are the same two main mechanisms through which these background events can satisfy the RS requirement imposed on the interaction events: either a second K_L^0 interacting simultaneously in the target or an initial "soft" interaction in the target followed by another interaction, downstream of the RS counters, which yields the two observed muons.

This source of background must be removed on a statistical basis, since at these relatively low energies the errors due to Coulomb scattering render the determination of the z vertex position insufficient to decide if the muon pair originated in the target. This is especially true for low-mass dimuons, and thus such a cut would seriously distort the mass spectrum. Accordingly, we shall estimate this contamination by studying those events which have two detected muons but no P, Q, R, or S counter latch. We recall here that these counters were not part of the hardware trigger but were only imposed in the logic requirement subsequently in software. In the subsequent discussion, we shall refer to the accepted sample of interaction events, i.e., events with an R or S (but no P or Q) as RS data and the events with two good muons, but no P, Q, R, or S shall be called $\overline{RS}$ data.

To the extent that the momentum spectrum of the K_L^0's yielding 2 μ's from an interaction point downstream of the RS counters is the same regardless whether an R or S counter fired or not, we can use the $\overline{RS}$ data to calculate the amount of the contamination under discussion in the RS data. More specifically, the ratio of the number of events eliminated by the VEND cut to those which pass the VEND cut but still occurring downstream of the RS counters will be the same in the RS data as in the $\overline{RS}$ data. The assumption about the near equality of the momentum spectrum is clearly rigorously true for the background events originating from the "accidentals" mechanism. That it is also quite good for the totality of the data is indicated by the similarity of the momentum spectrum of the dimuon system from the events eliminated by the VEND cut from the $\overline{RS}$ data to those eliminated by the same cut from the RS data.

Accordingly, to perform the subtraction, we have processed all the events without R and S counters in the same manner as those with R and/or S counters. Subsequently, we subtracted from the RS data the number of $\overline{RS}$ events passing all the interaction event cuts (except of course the requirement of pointing to a latched R or S counter), scaled by the ratio of number of events eliminated by the VEND cuts in the RS data sample to the number of events eliminated by that cut in the $\overline{RS}$ data sample. The results of this background subtraction are indicated on the second line in Table III, where the data have been separated into the runs with different target densities and into the low and high dimuon mass samples.

(3) hadrons simulating muons and (4) accidentals. We choose to discuss both of these sources together since the background events originating from them can be subtracted together on a statististical basis by using the like-sign dimuons. The fact that a majority of the like-sign dimuons are due to accidentals is illustrated in Fig. 7, displaying the measured time difference between the two observed muons. The like-sign dimuons

TABLE III. Background subtraction.

	Low mass $m_{\mu\mu} < 0.44$ GeV/c^2			High Mass $0.44 < m_{\mu\mu} < 1.22$ GeV/c^2		
	0 cm	4 cm	8 cm	0 cm	4 cm	8 cm
(a) Interaction events with RS, after VEND cut	131	116	82	120	91	68
(b) +- background calculated from $\overline{RS}$ data	34±3	17±2	17±2	8±1	4±1	3±1
(c) From ++/-- background	41±10	21±6	21±5	16±5	32±6	34±6
(d) Residual signal	55±16	78±13	44±11	96±12	55±12	31±10

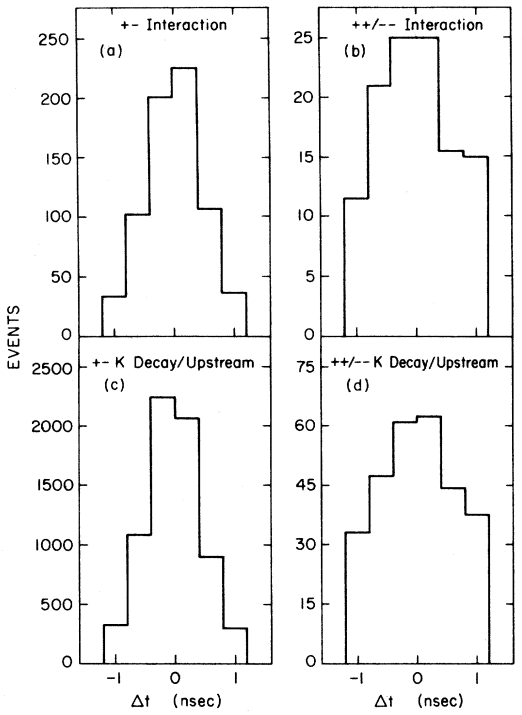

FIG. 7. Distribution in Δt between the two muons for (a) $+-$ interaction (b) $++/--$ interaction, (c) $+-$ K decay/upstream, and (d) $++/--$ K decay/upstream data before backgound subtractions.

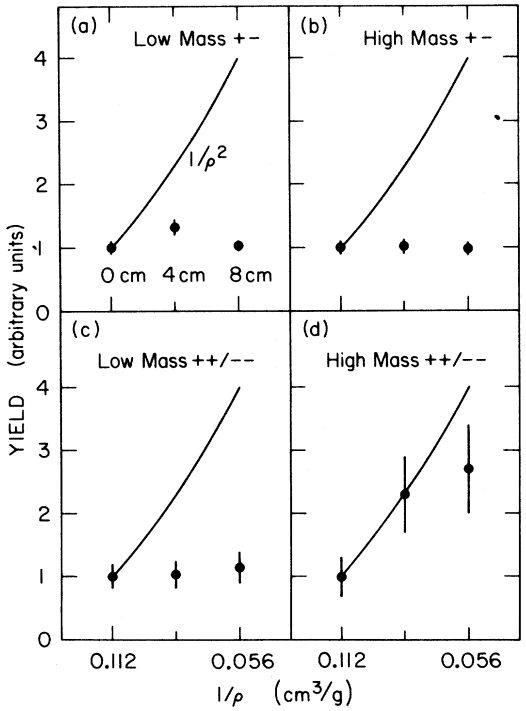

FIG. 8. The yield of interaction events, after correction for detection efficiency and normalized to the K_L^0 flux, is shown as a function of target density $1/\rho$, for (a) low mass $+-$, (b) high mass $+-$, (c) low mass $++/--$, and (d) high mass $++/--$ dimuon pairs. Also shown in each plot is the curve $1/\rho^2$.

show a much higher flat background than the unlike-sign dimuons which have a time distribution consistent with that expected for events with muons from the same K_L^0.

The contribution due to early hadron decays can be estimated by studying the number of observed events with different target densities. The yield of interaction events corrected for detection efficiency and normalized to the K_L^0 flux (as obtained from $K_{\mu 3}^0$ decays) is shown in Fig. 8 as a function of density for the 0-, 4-, and 8-cm data. The decay contamination should have a $(1/\rho)^2$ dependence due to the presence of two muons. The contribution due to decays is quite small as could have been argued *a priori* from the known $\pi^\pm$ and $K^\pm$ decay lifetimes. It is therefore reasonable to assume that the main sources of the like-sign muons are hadron punchthrough, or accidental time coincidences. Furthermore, these same mechanisms must also contribute to the unlike-sign muons.

Accordingly, we shall estimate the number of background interaction events due to these two sources by studying the like-sign muons satisfying all the interaction event criteria.

We first correct the numbers of like-sign dimuons for interactions occurring downstream of the S counters in the absorber by using the same procedure as described above for the unlike-sign dimuons. This gives us a number of like-sign dimuons produced at each density in the target region. At high energies, where the multiplicities are large, it is probably a reasonable assumption to take the number of unlike-sign muons due to these two background sources as equal to the number of like-sign muons. On the other hand, at our low energies and the resultant low multiplicities, the most reasonable assumption is that the punchthroughs will be due mainly to π's and K's, since protons tend to be emitted at low energies in the laboratory. Table IV lists the relative number of $+-$, $++$, and $--$ meson pairs that can be

TABLE IV. Relative rates of $+-$, $++$, $--$ $\mu\mu$ pairs.

	$+-$	$++$	$--$
Three-body final state	1	0	0
Four-body final state	13	2	2

TABLE V. P, Q, R, S inefficiency.

	P	Q	R	S	$\overline{PQ}\,RS$
Inefficiency	5.1%	2.9%	3.3%	1.8%	0.015%

produced in three- and four-body K^0N reactions, on the assumption that within each class all the channels are produced with equal probability. The much higher *a priori* probability of having two unlike-sign mesons as opposed to two like-sign mesons is quite apparent. Thus it appears imperative to deduce the ratio of like-sign to unlike-sign punchthroughs from the experimental data.

To this end, we again use the $\overline{RS}$ data. Ideally one should extrapolate the ratio of unlike- to like-sign dimuons observed in that sample as a function of the distance of the vertex from the target. Within our statistics and resolution this ratio appears constant as a function of Z with a value of about 2.5. We therefore used this factor to multiply the number of like-sign muon events to obtain the contamination among the unlike-sign muons due to hadron punchthroughs and accidental time coincidences. The numbers of events subtracted are shown in Table III, line (c). It should be emphasized here that the subtractions in Table III were performed on a mass bin basis, to allow for the different amount of each kind of contamination in each mass bin.

(5) K decays in front of P counter bank. In principle, the decay products of a K_L^0 decay occurring upstream of the P counter bank could fail to register in the P and Q counters and thus could simulate a low-mass interaction event. There are two independent ways to show that this contamination is negligible. We can first estimate the P and/or Q inefficiency by seeing what fraction of time the P misses when Q, R, S are present, or alternatively Q misses when P, R, S are present. These numbers are given in Table V together with the calculated probability that both P and Q miss. This calculated inefficiency leads to an expected background of one event, a result that is not surprising when one recalls that two charged particles are produced in each K_L^0 decay. An independent test of this small contamination is obtained by counting the number of events with $V \cdot \overline{P \cdot Q} \cdot R \cdot S$. The observed number of 17 is consistent with the calculated number of 18 accidental events obtained from the measured V rate.

The final mass plot after all of the subtractions have been performed is illustrated in Fig. 9. It exhibits two regions: (1) the low-mass dimuons with $m_{\mu\mu} < 0.5\,\mathrm{GeV}/c^2$, and (2) the dimuons presumably coming from the decay of the vector mesons. Furthermore, the backgrounds discussed above affect the low-mass part of the spectrum more than the high-mass (vector-meson decay) region. This is due mainly to two reasons. Firstly, the P_T distribution of the hadrons is such that any unsubtracted hadron punchthrough preferentially populates the low-mass region. Secondly, the measured mass of a high-mass pair produced in the absorber downstream of the RS counters would be systematically underestimated by falsely fitting a vertex to the target region. Accordingly, we would like to end this section by looking at two distributions that are sensitive to the presence of background to see if there is any evidence for residual contamination in the low-mass region.

One test of whether the low-mass dimuon events are due to genuine muons is the distribution of the deviations in the muon WSC's of the observed hits from the predicted hits, the latter based on extrapolating the track segments downstream of the

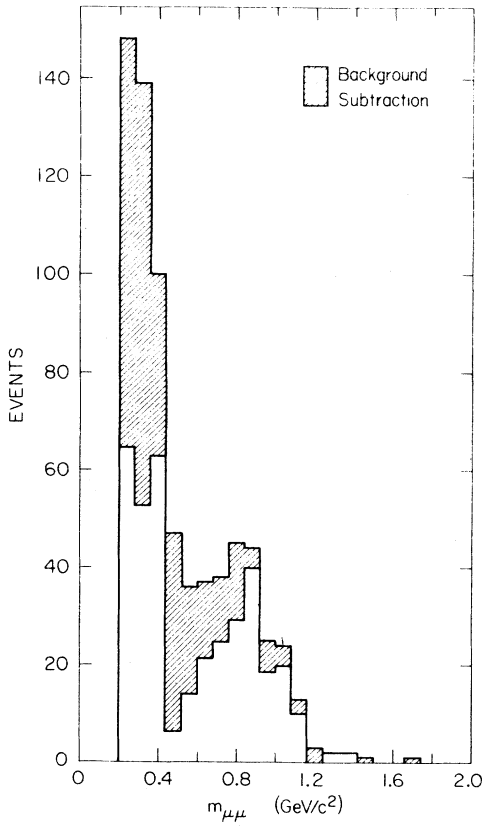

FIG. 9. Mass of $\mu^+\mu^-$ plotted in 0.4-GeV/c^2 bins after the VEND cut. The shaded area represents the calculated background subtraction as discussed in Sec. VI. The remaining events represent our final data sample before corrections for K decays in the target region and Bethe-Heitler pairs as discussed in Sec. VIII.

magnet through the lead absorber to the muon WSC's. This distribution, corrected for momentum dependence, is displayed in Fig. 10 for the high-mass events, K decays (both upstream and downstream of the V counter), residual events (after VEND cut) from the $\overline{RS}$ data, and the low-mass events remaining after the background subtraction. As can be seen from Fig. 10(c), which contains large amount of hadron punchthroughs, this distribution is quite sensitive to the presence of any nonmuonic background. The similarity between Fig. 10(d) and Figs. 10(a) and 10(b) leads us to believe that the low-mass dimuons represent a relatively pure sample.

As we saw earlier the distribution of the difference of measured times of the two muons is quite sensitive to any residual contamination from accidentals. Accordingly in Fig. 11 we compare the time difference distribution of the low-mass interaction events to the distributions of high-mass interaction events and of the K decays. Within statistics there is no evidence for any difference.

On the basis of these tests it appears to us highly unlikely that more than 15% of the low-mass dimuons could be due to sources other than genuine events occurring in the Cu target.

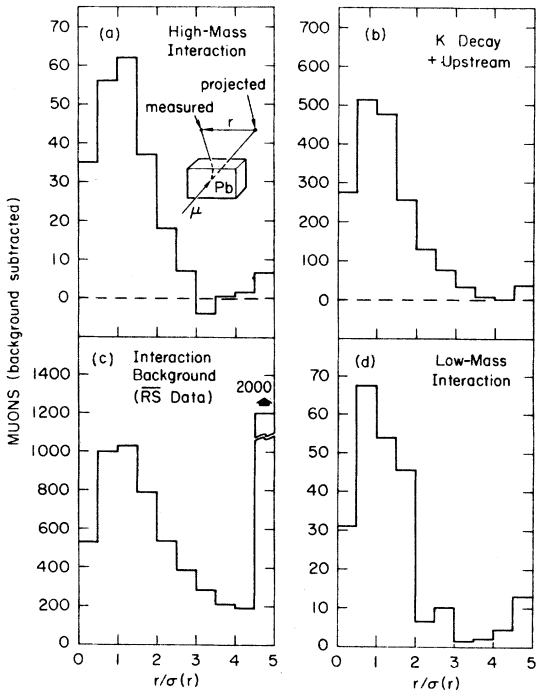

FIG. 10. Distribution in $R/\sigma(r)$ for (a) high-mass interaction events, (b) K decays, both upstream and downstream of V, (c) interaction events from $\overline{RS}$ data, and (d) low-mass interaction events. r is the distance between the projected and measured points in the muon WSC's. The last bin includes overflows. Backgrounds have been subtracted from plots (a), (b), and (d).

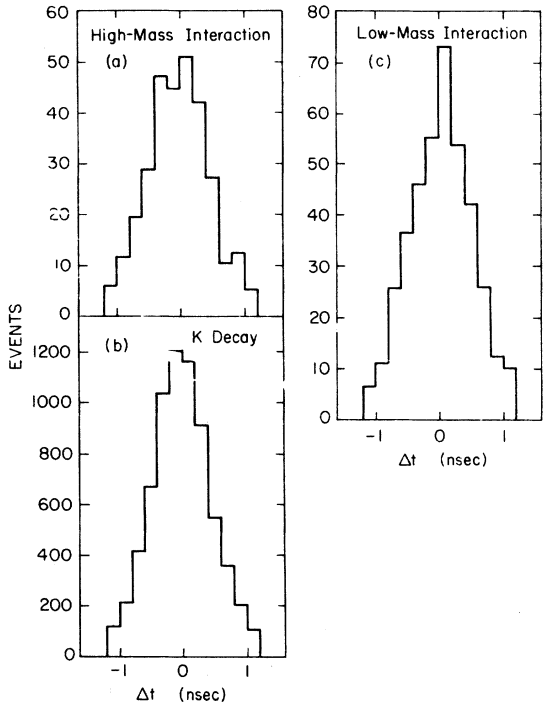

FIG. 11. Distribution in Δt between the two muons for (a) high-mass interaction events, (b) K decays, both upstream and downstream of V, and (c) low-mass interaction events. Backgrounds have been subtracted.

VII. INTERPRETATION OF THE MASS PLOT

The most natural interpretation of the high-mass ($m_{\mu\mu} > 0.5$ GeV/c^2) spectrum is in terms of the three well-known vector mesons: ρ, ω, and ϕ. Our resolution is insufficient to resolve the ρ-ω and ϕ peaks. Figure 12(a) indicates the Monte Carlo calculated distributions expected for pure ω, ρ, and Φ production, arbitrarily normalized to the same production cross section times branching ratio into μ pairs. For comparisons, Fig. 12(b) shows the expected dimuon spectrum resulting from K decays superimposed on the actual distribution. The fair agreement of the two illustrates the level of our understanding of the resolution. Finally, Fig. 12(c) illustrates the comparison of several different mixtures of the ρ, ω, and ϕ mesons with the actual high-mass data.

The presence of low-mass dimuon events in hadronic events has been somewhat of a mystery during the last few years. We would like to discuss next whether our experiment requires new

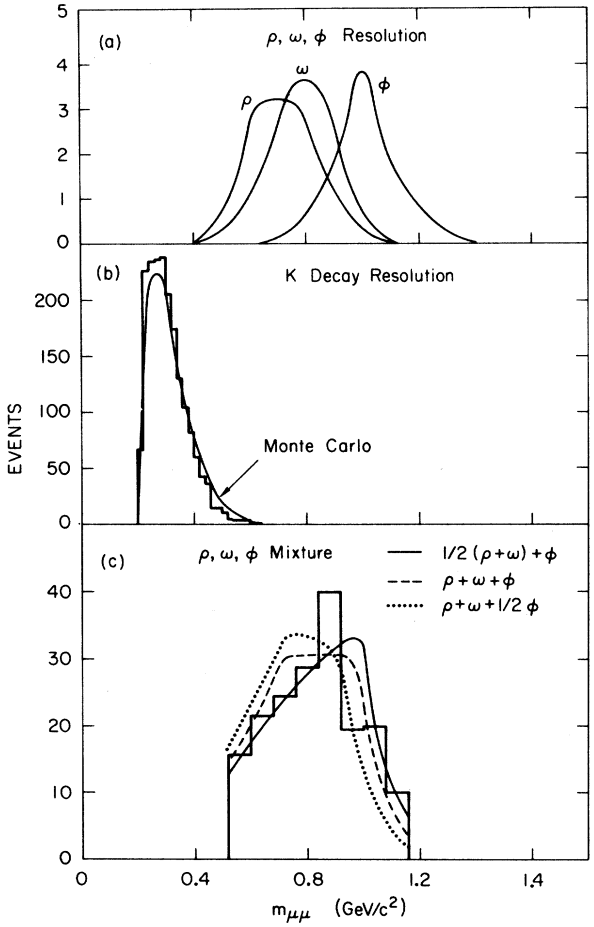

FIG. 12. (a) Resolution for ρ, ω, ϕ production, (b) observed $m_{\mu\mu}$ spectrum for $K_{\mu 3}^0$ decays followed by $\pi \to \mu\nu$ together with the expected Monte Carlo distribution, (c) observed high-mass dimuon spectrum and fits for various mixtures of ρ, ω, and ϕ.

sources to account for these dimuons, or whether they can be explained by the more conventional mechanisms, such as K decays in the Cu target, Bethe-Heitler pairs, or radiative decays of η and ω.

(a) *K decays.* A certain number of K_L^0's will decay in the Cu target between the Q and R counters, and will be followed either by pion decay before its interaction or by pion punchthrough. The calculation here is quite straightforward. We start by calculating the number of K decays at each density in the decay region, i.e., between the V and P counters. We correct for the small differences in the detection efficiency and the decay pathlengths for the K and π at each density. The absorption length in Cu is taken to be 15 cm when calculating the π and K flight path. We also assumed a 10^{-3} pion punchthrough probability which is our estimate of the total probability for a pion to fake a muon by all the possible mechanisms. On the basis of a previous experiment[30] with this apparatus, we believe this estimate to be good to 50%. The fact that this probability can only be estimated with a large uncertainty is not too important since it only contributes less than 10% to the total "decay" process. The raw and corrected numbers are shown in Table VI. The K decays with like-sign muons are predominantly two K_L^0 decays accidentally in time (see Fig. 7).

Using now the flux, as determined above, we can calculate the number of events for each density where either both decays (i.e., K_L^0 and π) occur after the Q counter, or the K_L^0 decays after Q counter and the π manages to penetrate through the Cu block. The pion penetration accounts now for 50% of these events at high density and 34% at low density, so this background calculation is more sensitive to the pion penetration level than the flux calculation. The calculated numbers of these events are shown in Table VII, line (b).

(b) *ω decays.* To estimate the number of potential $\mu^+\mu^-$ pairs originating from $\omega \to \pi^0\mu^+\mu^-$ decays we have used the following input[31]:

(i) $R = (\omega \to \pi^0\mu^+\mu^-)/(\omega \to \mu^+\mu^-) = 0.64$;

(ii) one quarter of all high-mass dimuon events are due to ω's;

(iii) the relative efficiency for detection $\omega \to \pi^0\mu^+\mu^-$ to $\omega \to \mu^+\mu^-$ as calculated by Monte Carlo is 0.5.

The calculated numbers for each density are shown in Table VII, line (c).

(c) *η decays.* The best theoretical estimates

TABLE VI. K decay normalization.

	N_{+-}	$N_{++/--}$	$N=N_{+-}-N_{++/--}$	Relative detection efficiency	Relative decay efficiency	Corrected N
0 cm	700	37	663	1.0	1.0	633
4 cm	519	20	499	0.889	0.927	608
8 cm	439	19	420	0.833	0.853	592

TABLE VII. Calculated sources of low-mass dimuons. The contribution from $\eta \to \mu^+\mu^-\gamma$ is discussed in Sec. VII C.

	0 cm	4 cm	8 cm
(a) Low-mass signal	55 ± 16	78 ± 13	44 ± 11
(b) K decays	11 ± 6	16 ± 7	22 ± 8
(c) ω decay	6	4	4
(d) Bethe-Heitler I	73	51	48
(e) Bethe-Heitler II	13	9	9

give[32]

$$\frac{\eta \to \mu^+\mu^-\gamma}{\eta \to \text{all}} = 2.85 \times 10^{-4}.$$

Combined with the experimental measurement of[33]

$$\frac{\eta \to \mu^+\mu^-}{\eta \to \text{all}} = (2.2 \pm 0.8) \times 10^{-5}$$

and the relative Monte Carlo detection efficiency of 2.5 in favor of the two-body decay, this leads to the conclusion that we should see about $5\eta \to \mu^+\mu^-\gamma$ events for every $\eta \to \mu^+\mu^-$. Even though no $\eta \to \mu^+\mu^-$ peak exists in our data, we could not exclude the existence of 15–20 events of this type, or 75–100 events from $\eta \to \mu^+\mu^-\gamma$, enough to explain the remaining low-mass events. It remains to ask what that would imply about the total η production rate. Again on the basis of our Monte Carlo calculation and assuming that

$$B_{\rho \to 2\mu}\sigma_\rho = B_{\omega \to 2\mu}\sigma_\omega = \tfrac{1}{2}B_{\phi \to 2\mu}\sigma_\phi,$$

this would imply that η's are produced at a rate comparable to that of the ω mesons. We know of no data which either support or contradict this production rate. We can only note for reference that in K^-p interactions at lower energies the exclusive ω production channels tend to be a factor of 3–5 higher than the corresponding η channels.[34]

(d) *Bethe-Heitler Processes.* We should consider here two sources of parent γ rays which then could convert to $\mu^+\mu^-$ pairs, namely γ rays from π^0's arising from $K_L^0 \to 3\pi^0$ decays, and γ rays from π^0's produced in K_L^0-Cu interactions. The first source has been shown to be completely negligible (< 0.1 event) based on Monte Carlo studies. To estimate the second source of potentail background, we start by assuming that the x_F and P_T distributions for the inclusive π^0 production by K_L^0's in our energy range is the same as that of π^-'s in K^-p interactions at 32 GeV/c.[35] This is a reasonable guess, since the charges of the pions in both cases correspond to the charge of the incoming K, and the K^- energy is only a factor of 3.5 above the mean energy of K_L^0's producing our detected muons. Furthermore, we take the average π^0 multiplicity to be 1.6, i.e., the same as π^- multiplicity quoted in Ref. 35. Combining this with the probability that a γ converts to a $\mu^+\mu^-$ pair as calculated by Tsai,[36] we arrive at the contributions due to the Bethe-Heitler process indicated in Table VII, line (d). On the other hand, if we use the x_F and P_T distributions as given in equation (1), we obtain the Bethe-Heitler contributions shown in Table VII, line (e). Thus the Bethe-Heitler contribution to the low-mass events is highly uncertain due to its high sensitivity on the production dynamics in the high x_F region for $K^0N \to \pi^0X$.

VIII. CONCLUSION

Muon pairs have been observed in K_L^0 interactions and they fall into two categories: low mass ($m_{\mu\mu} < 0.5$ GeV/c^2) and high mass ($m_{\mu\mu} > 0.5$ GeV/c^2) corresponding to vector-meson decays. Using reasonably orthodox assumptions one can conclude that there is no need to invoke any new sources to explain the observed dimuon production. Alternatively, if one tries to add up the minimum required contributions to the low-mass muon pairs from the known sources, e.g., K decays, ω radiative decays, the Bethe-Heitler processes, we can set an upper limit on the production cross section of new-source low-mass muon pairs with $x_F > 0.25$ of 20 nb per nucleon. In deriving this upper limit we have used our Bethe-Heitler calculation from Table VII(e), taken the η production cross section to be negligible, and assumed that the production cross section for μ pairs has the same A dependence as the total K_L^0 cross section. We choose to quote the cross section for $x_F > 0.25$ since for our K_L^0 momentum spectrum the detection efficiency for muon pairs falls to zero below the value, due to the requirement that the muons penetrate the full length of the Cu and Pb absorbers.

This upper limit of 20 nb can be compared with the preliminary data from the experiment performed with the SLAC streamer chamber studying dimuon production in 16-GeV/c πp interactions.[37] Owing to their better mass resolution and negligible Bethe-Heitler background, they are able to argue that the observed low-mass dimuon pairs have a broader spectrum than that expected from ω and η Dalitz decays. They conclude that they observe an excess of events (not accounted by these decays) with a production cross section of about 50 nb for $x_F > 0.3$. For comparison, we note that Anderson *et al.*[23] find a cross section of 140 ± 30 nb for the production of all dimuon pairs in πp interactions at 150 GeV/c with $x_F > 0.3$ in

the range $0.21 < m_{\mu\mu} < 0.45$ GeV/c^2.

Our resolution is not good enough to resolve the three neighboring vector mesons ρ, ω, and ϕ. The mass spectrum is fitted well by assuming that

$$B_{\rho\to 2\mu}\sigma_\rho = B_{\omega\to 2\mu}\sigma_\omega = \tfrac{1}{2}B_{\phi\to 2\mu}\sigma_\phi,$$

where $B_{V\to 2\mu}$ is the branching ratio of a given vector meson into muon pairs, and σ_V is the production cross section of that vector meson integrated over our K_L^0 spectrum.[38] The assumed production angular distribution for $x_F > 0$,

$$\frac{d\sigma}{dx_F dP_T^2} \propto (1-x_F)^3 e^{-4.2P_T^2},$$

appears to fit the data reasonably well. The cross section per nucleon for high-mass $\mu\mu$ pair production with $x_F > 0.25$ is 55 ± 10 nb per nucleon. Again, we assume the same A dependence for $\mu\mu$ pair production as for the total K^0 cross section.

Even though our acceptance (see Fig. 5) decreases rapidly at high masses, we still retain some sensitivity at the $\psi(3100)$. No events were observed in this vicinity. Averaged over our K_L^0 momentum spectrum, this gives an upper limit on $B_{\psi\to 2\mu}\sigma_\psi(x_F > 0.25)$ of 35 nb per nucleon at a 90% confidence level. This upper limit was calculated by application of the same production model as the lower-mass vector mesons.

ACKNOWLEDGMENTS

We thank R. Coombes, D. Hitlin, D. Porat, and C. Rasmussen for their contributions to this experiment. We also acknowledge the excellent support of the Accelerator Operations, Experimental Facilities, and Computer Operations groups of the Stanford Linear Accelerator Center. This work was supported in part by the United States National Science Foundation and by the United States Energy Research and Development Administration.

---

*Current address: CERN, Geneva, Switzerland.
†Currently with American Asian Bank, San Francisco, California.
‡Current address: Hughes Aircraft, Newport Beach, California.
§Current address: Systems Control, Inc., Palo Alto, California.

[1]R. C. Lamb *et al.*, Phys. Rev. Lett. 15, 800 (1965); R. Burns *et al.*, *ibid.* 15, 830 (1965).
[2]Y. Yamaguchi, Nuovo Cimento 43, 193 (1966).
[3]P. J. Wanderer *et al.*, Phys. Rev. Lett. 23, 729 (1969).
[4]L. M. Lederman *et al.*, Phys. Rev. Lett. 25, 1523 (1970); see also A. Wehmann *et al.*, *ibid.* 17, 1113 (1966) and B. Hyams *et al.*, Phys. Lett. 24B, 634 (1967).
[5]S. D. Drell and T.-M. Yan, Phys. Rev. Lett. 25, 316 (1970).
[6]J. P. Boymond *et al.*, Phys. Rev. Lett. 33, 112 (1974); J. A. Appel *et al.*, *ibid.* 33, 722 (1974); D. Bintinger *et al.*, *ibid.* 35, 72 (1975).
[7]J. J. Aubert *et al.*, Phys. Rev. Lett. 33, 1404 (1974); J.-E. Augustin *et al.*, *ibid.* 33, 1406 (1974).
[8]G. S. Abrams *et al.*, Phys. Rev. Lett. 33, 1453 (1974).
[9]H. D. Snyder *et al.*, Phys. Rev. Lett. 36, 1415 (1976); M. Binkley *et al.*, *ibid.* 37, 574 (1976); K. J. Anderson *et al.*, *ibid.* 36, 237 (1976).
[10]S. L. Glashow, J. Iliopoulos, and L. Maiani, Phys. Rev. D 2, 1285 (1970).
[11]G. R. Farrar and S. C. Frautschi, Phys. Rev. Lett. 36, 1017 (1976).
[12]P. Darriulat *et al.*, paper presented at the XVIII International Conference on High Energy Physics, Tbilisi, 1976 (unpublished); see also E. Beier *et al.*, Phys. Rev. Lett. 37, 1114 (1976).
[13]H. Kasha *et al.*, Phys. Rev. Lett. 36, 1007 (1976); K. J. Anderson *et al.*, *ibid.* 37, 803 (1976).
[14]B. A. Dolgoshein, in *Proceedings of the XVIII International Conference on High Energy Physics, Tbilisi, 1976*, edited by N. N. Bogolubov *et al.* (JINR, Dubna, U.S.S.R., 1977), Vol. II, p. B157.
[15]L. Leipuner *et al.*, Phys. Rev. Lett. 36, 1011 (1976); M. J. Lauterbach *et al.*, *ibid.* 37, 1436(C) (1976).
[16]N. Z. Anisimova *et al.*, Phys. Lett. 65B, 85 (1976).
[17]D. M. Grannan *et al.*, Phys. Lett. 69B, 125 (1977).
[18]L. B. Leipuner *et al.*, Phys. Rev. Lett. 35, 1613 (1975); D. Bucholz *et al.*, *ibid.* 36, 932 (1976).
[19]L. B. Leipuner *et al.*, Phys. Rev. Lett. 34, 103 (1975); K. Winter, Phys. Lett. 57B, 479 (1975).
[20]See for example D. Hitlin, Proceedings of the Summer Institute on Particle Physics, Report No. SLAC-198, 1976 (unpublished); P. Piroué, in *Particles and Fields '76*, proceedings of the Annual Meeting of the Division of Particles and Fields of the APS, Brookhaven National Laboratory, edited by H. Gordon and R. F. Peierls (BNL, Upton, New York, 1977), p. A1; L. M. Lederman, Phys. Rep. 26C, 149 (1976).
[21]L. Baum *et al.*, Phys. Lett. 60B, 485 (1976).
[22]E. Beier *et al.*, Phys. Rev. Lett. 37, 1117 (1976); A. Browman *et al.*, *ibid.* 37, 246 (1976).
[23]K. J. Anderson *et al.*, Phys. Rev. Lett. 37, 799 (1976).
[24]G. Goldhaber *et al.*, Phys. Rev. Lett. 37, 255 (1976).
[25]A. Benvenuti *et al.*, Phys. Rev. Lett. 34, 419 (1975); 35, 1199 (1975); B. C. Barish *et al.*, *ibid.* 36, 939 (1976); J. van Krogh *et al.*, *ibid.* 36, 710 (1976).
[26]W. Braunschweig *et al.*, Phys. Lett. 63B, 471 (1976).
[27]D. Bintinger *et al.*, Phys. Rev. Lett. 37, 732 (1976); M. A. Abolins *et al.*, *ibid.* 37, 417 (1976).
[28]R. Piccioni *et al.*, Phys. Rev. D 9, 2939 (1974).
[29]L. Eyges, Phys. Rev. 74, 1534 (1948).
[30]G. Donaldson *et al.*, Phys. Rev. D 9, 2960 (1974).
[31]C. H. Lai and C. Quigg have estimated the relative branching ratio $\Gamma(\omega\to\pi^0\mu^+\mu^-)/\Gamma(\omega\to\pi^0\gamma)$ as 5.5. Quoted in K. J. Anderson *et al.*, Phys. Rev. Lett. 37, 799 (1976).
[32]C. Jarlskog and H. Pilkuhn, Nucl. Phys. B1, 264 (1967).
[33]B. D. Hyams *et al.*, Phys. Lett. 29B, 128 (1969).

[34]J. Mott *et al.*, Phys. Rev. 177, 1966 (1969); Birmingham-Glasgow-London (I.C.) Oxford-Rutherford Collaboration, *ibid.* 152, 1148 (1966).
[35]M. Faccini *et al.*, Saclay report, 1977 (unpublished).
[36]Y.-S. Tsai, private communication. Also, see Rev. Mod. Phys. 46, No. 4, 815 (1974).
[37]K. Bunnell *et al.*, paper presented to the 1977 International Symposium on Lepton and Photon Interactions at High Energies, West Germany (unpublished).
[38]A similar result has been obtained in K^-Be interactions at 42 GeV/c by Y. M. Antipov *et al.*, paper presented at the XVIII International Conference on High Energy Physics, Tbilisi, 1976 (unpublished).